

# Carbon Monoxide Mediated Hydrogen Release from PtCu Single-Atom Alloys: The Punctured Molecular Cork Effect

*Matthew T. Darby<sup>1</sup>, Felicia R. Lucci<sup>2</sup>, Matthew D. Marcinkowski<sup>2</sup>, Andrew J. Therrien<sup>2</sup>, Angelos Michaelides<sup>3</sup>, Michail Stamatakis<sup>1\*</sup> and E. Charles H. Sykes<sup>2\*</sup>*

## **Author Information**

- 1 Thomas Young Centre and Department of Chemical Engineering, University College London, Roberts Building, Torrington Place, London, WC1E 7JE, UK
- 2 Department of Chemistry, Tufts University, 62 Talbot Avenue, Medford, Massachusetts 02155, United States
- 3 Thomas Young Centre, London Centre for Nanotechnology and Department of Physics and Astronomy, University College London, 17-19 Gordon Street, London, WC1E 6BT, UK

## **Corresponding Author**

\*E-mail: [charles.sykes@tufts.edu](mailto:charles.sykes@tufts.edu), [m.stamatakis@ucl.ac.uk](mailto:m.stamatakis@ucl.ac.uk)

**Abstract:** Pt based materials are used extensively in heterogeneous catalytic processes, but are notoriously susceptible to poisoning by CO. In contrast, highly dilute binary alloys formed of isolated Pt atoms in a Cu metal host, known as PtCu single-atom alloys (SAAs), are more resilient to CO poisoning during catalytic hydrogenation reactions. In this article, we describe how CO affects the adsorption and desorption of H<sub>2</sub> from a model PtCu(111) SAA surface and gain a microscopic understanding of their interaction at the Pt atom active sites. By combining temperature programmed desorption and scanning tunneling microscopy with first principles kinetic Monte Carlo we identify CO as a Pt site blocker that prevents the low temperature adsorption and desorption of H<sub>2</sub>, the so-called *molecular cork effect*, first realized when examining PdCu SAAs. Intriguingly, for the case of PtCu, H<sub>2</sub> desorption occurs before CO release is detected. Furthermore, desorption experiments show a non-linear relationship between CO coverage of the Pt sites and H<sub>2</sub> desorption peak temperature. When all the Pt atoms are saturated by CO a very sharp H<sub>2</sub> desorption feature is observed 55 K above the regular desorption temperature of H<sub>2</sub>. Our simulations reveal that the origin of these effects is the fact that desorption of just one CO molecule from a Pt site facilitates the fast release of many molecules of H<sub>2</sub>. In fact, just 0.7 % of the CO adsorbed at Pt sites has desorbed when the H<sub>2</sub> desorption peak maximum is reached. The release of H<sub>2</sub> from CO corked PtCu SAA surfaces analogous to the escape of gas from a pressurized container with a small puncture. Given that small changes in CO surface coverage lead to large changes in H<sub>2</sub> evolution energetics the *punctured molecular cork effect* must be considered when modeling reaction mechanisms on similar alloy systems.

## Introduction

CO is a common catalytic poison, especially for Pt based heterogeneous catalysts.<sup>1-3</sup> The strong adsorption energy of CO on Pt hinders the dissociation and recombination of H<sub>2</sub> via Pt sites.<sup>2</sup> Furthermore, H<sub>2</sub> and CO are key species in a great number of catalytic conversions in the energy industry, including Fischer-Tropsch synthesis, methane steam reforming, and methanol/ethanol fuel cells. Often, the interaction between surface bound H and CO is repulsive, which can impact the uptake and release of both species from the metal surface.<sup>4-11</sup> Thus, a fundamental understanding of the interactions between H, CO and the substrate must not be overlooked in the rational design of new catalysts.

In previous work, it has been shown that the co-adsorption of H and CO on bimetallic alloys produces unique desorption behavior. On PdCu(111) single-atom alloys (SAAs), CO raises the desorption temperature of H<sub>2</sub>, allowing H adatoms that have spilled over from the Pd sites to Cu to remain on the surface beyond the normal desorption temperature, a phenomenon known as the *molecular cork effect*.<sup>12</sup> Similar behavior has been reported on Pd<sub>70</sub>Au<sub>30</sub> bimetals, where adsorbed CO traps H in the near-surface layer.<sup>13</sup> In contrast, on PdAu SAAs, H<sub>2</sub> desorbs from the surface at a lower temperature in the presence of CO as it is forced by CO onto the Au(111) host from which it desorbs at 110 K.<sup>14</sup> This is also observed on Co nanoparticles supported on Cu(111) where CO exerts a two-dimensional pressure forcing H off the Co islands onto the Cu(111) surface.<sup>10</sup> These studies show that both the atomic scale surface structure and the nature of the adsorbed species impact the H<sub>2</sub> desorption temperature. In this study, we further the understanding of co-adsorption of CO and H on SAAs by studying PtCu alloys. We have previously found that PtCu SAAs exhibit enhanced reaction selectivity, stability, and tolerance to

CO poisoning as compared to monometallic catalysts;<sup>15-17</sup> therefore, they represent promising candidates for overcoming the current limitations of Pt-based catalysts.

To understand the fundamentals of CO interaction with isolated Pt atoms in Cu, as well as the effect on co-adsorbed H, we study the behavior of H and CO on a well-defined PtCu SAA model system. Using a combination of temperature programmed desorption (TPD) and scanning tunneling microscopy (STM) we probe the system to elucidate the energetics of H<sub>2</sub> adsorption and desorption, as well as the effect of co-adsorbed CO. We show that individual, isolated Pt atoms in the Cu(111) surface enable facile H<sub>2</sub> dissociation at low temperatures and spillover to majority Cu sites. Even though CO blocks H<sub>2</sub> dissociation and uptake at low temperatures, we show in the case of pre-adsorbing H prior to CO exposure that H<sub>2</sub> can desorb from the surface in the presence of CO, albeit at higher temperature than in the absence of CO. Furthermore, we also show that the H<sub>2</sub> peak temperature is dependent on the surface coverage of CO. Our experimental observations are explained using density functional theory (DFT) calculations and kinetic Monte Carlo (KMC) simulations, which we use to elucidate the mechanism of H<sub>2</sub> desorption from the PtCu(111) SAA surface in the absence versus in the presence of CO, and model the kinetics of H<sub>2</sub> and CO TPD. Our simulations show that CO preferentially adsorbs at, and subsequently blocks, single Pt atom sites in the PtCu(111) SAA, preventing low temperature H-H recombination in a manner similar to a *molecular cork*. In contrast to the PdCu(111) SAA, H is held to higher temperature on the PtCu(111) SAA surface. This facilitates rapid H-H recombination when only a small fraction of Pt sites are free. When all the Pt sites are initially blocked by CO and the surface reaches a temperature allowing only 0.7% of the CO to desorb from the Pt sites, the H-H recombination rate is so high that the H<sub>2</sub> peak maximum occurs, analogous to the release of gas from a punctured balloon. Finally, we show with KMC

simulations that there is a non-linear dependence of the H<sub>2</sub> desorption peak temperature on initial CO coverage on Pt. Initial coverages of 99.8% (just 0.2% lower than full coverage, corresponding to only one free Pt atom) are enough to facilitate low temperature H<sub>2</sub> desorption. While the above discussion may suggest that PtCu SAAs are susceptible to poisoning by CO, CO in fact binds more weakly to Pt sites on the SAA, desorbing at 350 K as compared to ~450 K on pure Pt.

## Experimental Methods

TPD experiments were performed in an ultra-high vacuum (UHV) system with a base pressure of  $< 1 \times 10^{-10}$  mbar. The chamber was equipped with a quadrupole mass spectrometer (Hiden) and had the ability to cool the sample to 85 K with liquid nitrogen and resistively heat to 750 K. Surfaces were exposed to H<sub>2</sub> (99.9% Airgas) and CO (99.99% Airgas) by backfilling the chamber to the required pressure through high-precision leak valves while the sample was held at 85 K. Exposures are quoted in Langmuirs ( $1 \text{ L} = 1 \times 10^{-6}$  torr·s). TPD measurements were performed with a linear heating ramp of  $1 \text{ K} \cdot \text{s}^{-1}$ . Pt coverages were quantified by CO titration by saturating with CO (10 L) and taking ratios of CO desorption from Pt sites ( $>300 \text{ K}$ ) vs. Cu ( $<250 \text{ K}$ ), accounting for CO binding 1-to-1 atop to isolated Pt atoms in Cu<sup>12, 18-19</sup> and for the known saturation packing density of CO on Cu(111) (0.52 ML).<sup>20</sup>

STM experiments were performed using a low-temperature (LT) scanning tunneling microscope (Omicron Nanotechnology). The vacuum chambers had base pressures  $< 5 \times 10^{-11}$  mbar. In order to observe adsorbed H atoms, imaging was conducted at 5 K after exposure to H<sub>2</sub> at 85 K and subsequent cooling to 5 K. STM imaging of H adatoms occurred at non-perturbative tunneling conditions at or below 30 pA and 30 mV.<sup>21-22</sup>

## Computational Methods

We performed periodic, planewave DFT total energy minimization calculations using the Vienna *Ab Initio* Simulation Package (VASP) version 5.4.1<sup>23-24</sup> with the projector augmented wave (PAW) method<sup>25-26</sup> to model core ionic potentials and the revised Perdew-Burke-Ernzerhof (RPBE) exchange-correlation functional.<sup>27-28</sup> We note here that energies derived from DFT calculations are highly dependent on the choice of functional. In this case, we employed RPBE because it was designed specifically to overcome issues of over-binding encountered when using other xc-functionals. Our previous work showed that RPBE gives CO adsorption energies comparable to experimental results on both pure metal and SAA surfaces.<sup>29</sup> Our slab calculations used a  $3 \times 3 \times 5$  unit cell where ions in the top-most three layers were free to relax whereas those in the bottom two layers were fixed to the RPBE bulk FCC lattice constant for Cu (3.64 Å). In the case of PtCu SAA calculations, a single atom of Cu in the surface layer of the slab was replaced by Pt. A vacuum region of 10 Å was used to minimize periodic interactions in the z-direction. We used an  $8 \times 8 \times 1$  Monkhorst-Pack k-point mesh to sample the Brillouin zone and the planewave kinetic energy cutoff was set to 400 eV. To aid with convergence, we employed Methfessel-Paxton smearing with a smearing width set to 0.1 eV. We ensured electronic self-consistency up to a tolerance of  $10^{-7}$  eV and during ionic relaxation, we performed conjugate gradient minimization of the Hellmann-Feynman forces on free atoms to within a tolerance of  $10^{-2}$  eV·Å<sup>-1</sup>. To locate transition states we utilized the dimer method of Jónsson and Henkelman in VASP Transition State Tools version 3.1.<sup>30</sup> We confirmed that the transition states correspond to 1<sup>st</sup> order saddle points on the potential energy surface through vibrational frequency analysis using finite displacements of 0.02 Å. Adsorption energies ( $E_{ads}$ ) of H and CO are calculated relative to H<sub>2</sub> (g) and CO (g) such that

$$E_{ads} = E_{Tot}^{slab} - E_{Tot}^{clean} - \frac{m}{2} \cdot E_{Tot}^{H_2(g)} - n \cdot E_{Tot}^{CO(g)}, \quad (1)$$

where  $E_{Tot}^{slab}$  and  $E_{Tot}^{clean}$  are the DFT total energies of the slab with  $m$  H and  $n$  CO present and the clean slab, respectively.  $E_{Tot}^{H_2(g)}$  and  $E_{Tot}^{CO(g)}$  are the DFT total energies of isolated gas phase molecules of H<sub>2</sub> and CO, respectively. Note that more negative values of H and CO adsorption energies correspond to more stable binding.

Parameterized by our DFT calculations, we performed KMC simulations within the graph-theoretical framework as implemented in *Zacros*, version 2.0.<sup>31-33</sup> Rate constants  $k_{TST}$  for adsorption, desorption, surface diffusion and surface reactions were calculated according to transition state theory (TST):<sup>34</sup>

$$k_{TST} = \frac{k_B \cdot T}{h} \cdot \frac{Q^{TS}}{Q^{IS}} \cdot \exp\left(-\frac{\Delta E_a}{k_B \cdot T}\right) \quad (2)$$

where  $k_B$  is the Boltzmann constant,  $h$  is Planck's constant,  $T$  is the temperature,  $Q^{TS}$  and  $Q^{IS}$  are the molecular partition functions for the transition state and initial state, respectively, and  $\Delta E_a$  is the activation barrier. In order to compute the molecular partition functions  $Q$ , we used vibrational frequencies computed with DFT under the harmonic approximation. For non-activated adsorption events (e.g. CO adsorption) we assumed 2D gas behavior, as the reaction coordinate is identical to the third translational degree of freedom, perpendicular to the surface.<sup>34</sup> The pre-exponential factor in (2) is temperature dependent, both due to the thermal factor of  $k_B \cdot T/h$ , but also because  $Q^{TS}$  and  $Q^{IS}$  are functions of  $T$ :<sup>34</sup> this is accounted for in the KMC

simulation using fitted functions of  $T$ . Further information on the computation of  $k_{TST}$  using DFT calculations can be found in the supporting information of ref 34.

All KMC simulations utilized a  $50 \times 50$  hexagonal fcc(111) lattice with 5000 metal atoms (5000 top sites, 5000 fcc sites and 5000 hcp sites). For PtCu(111) SAA simulations, a Cu(111) lattice was used, where host metal sites were randomly substituted with dopant metal sites under the condition that these Pt sites cannot be first or second nearest neighbors. The Pt atom percentage density used in all simulations was approximately 10 %, which is comparable to that on model PtCu(111) SAA terraces within 10 nm of a step-edge.<sup>16, 35</sup>

Our simulations considered the following reversible elementary events (see schematics in supporting information): CO adsorption/desorption on Pt top sites and Cu three-fold hollow sites; H<sub>2</sub> dissociative adsorption/associative desorption on shared Pt-Cu-Cu fcc and hcp site second nearest neighbor pairs and Cu fcc and hcp site 1<sup>st</sup> nearest neighbor pairs; CO diffusion between Cu three-fold hollow sites as well as between Cu three-fold hollow sites and Pt top sites; H adatom diffusion between Cu three-fold hollow sites, Cu three-fold hollow sites and Pt-Cu-Cu three-fold hollow sites, and finally between Pt-Cu-Cu three-fold hollow sites. Kinetic parameters for all of these events were computed using harmonic TST and DFT calculated vibrational frequencies. We note that H adatom diffusion was treated as a fast quasi-equilibrated process and the kinetic constants thereof are scaled-down (“stiffness scaling”) whilst preserving this equilibrium in order to gain computational efficiency;<sup>36-37</sup> no other rate constants are scaled.

Finally, we simulated TPD using KMC by initializing the surface with H and/or CO at various coverages given in ML (where 1 ML = total number of surface metal atoms) and ramped the temperature uniformly at a rate of 1 K·s<sup>-1</sup>. The partial pressures of gas phase H<sub>2</sub> and CO were set



to zero in order to reproduce ultra-high vacuum conditions. Ensembles of 8 simulations with different initial random number seeds were used and were averaged to give the final TPD spectra.

## **Results and Discussion**

### **H<sub>2</sub> Activation and Desorption Kinetics with and without Co-adsorbed CO**

To directly probe the interaction of CO and H with isolated Pt atoms in the Cu(111) surface, we prepared PtCu SAAs by depositing low concentrations of Pt onto Cu(111) at 380 K. We have previously shown that, at these low Pt concentrations, Pt atoms exist as single isolated atoms in the surface layer of Cu.<sup>16,35</sup> The high dispersion of Pt in Cu allows us to selectively probe the interactions of H and CO at isolated Pt atoms. PtCu SAAs exhibit unique H<sub>2</sub> adsorption and desorption behavior as compared to monometallic surfaces.<sup>15-16</sup> Our previous TPD studies show that H<sub>2</sub> desorbs from PtCu SAAs at 230 K,<sup>15-17</sup> 70 K lower than the desorption temperature from either bare Cu(111)<sup>38</sup> or Pt(111) (~300 K).<sup>39</sup> This is explained by our DFT calculations, which reveal that isolated Pt atoms in Cu reduce the barrier for dissociative adsorption/recombination of H<sub>2</sub> relative to Cu(111). Additionally, the binding strength of H adatoms on PtCu SAAs are much weaker compared to Pt(111). Using DFT with the functional and parameters detailed in the experimental section, we compute the activation barrier for H<sub>2</sub> dissociation over a single Pt atom in the PtCu(111) SAA to be 0.09 eV, which is 0.66 eV lower than on Cu(111) (0.75 eV). Hence, we observe facile activation of H<sub>2</sub> on PtCu SAAs at temperatures as low as 85 K. Moreover, we compute a desorption barrier from PtCu(111) SAA of 0.39 eV, facilitating low temperature H-H recombination (230 K).

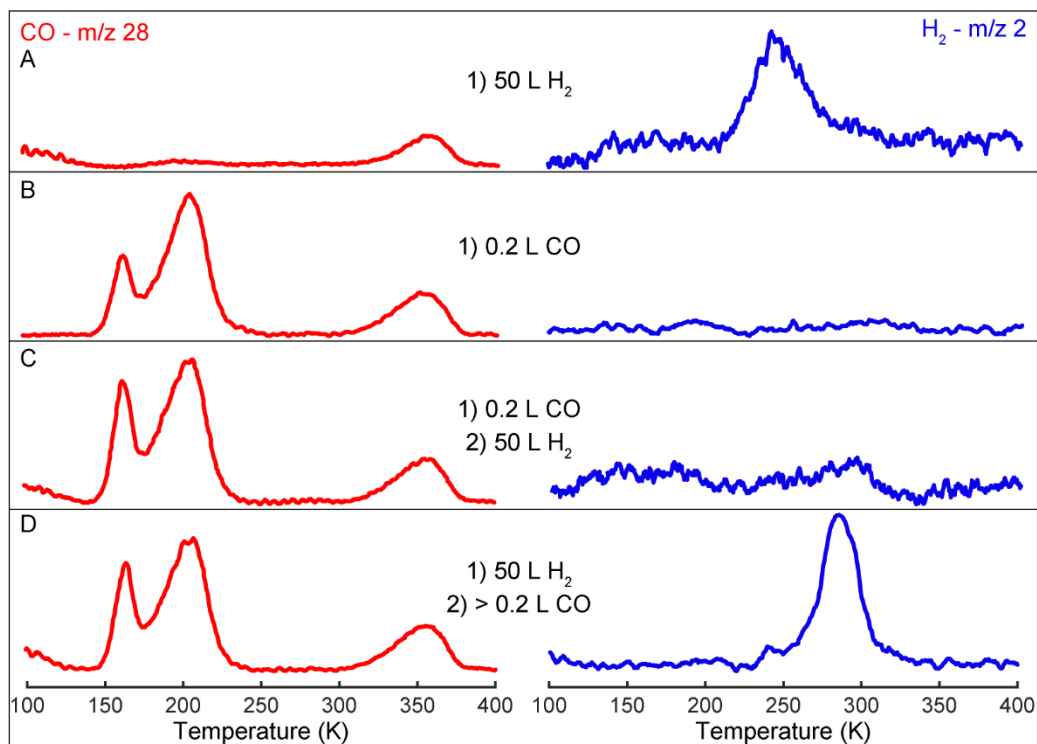


**Figure 1.** Co-adsorption of H and CO on PtCu(111) SAAs (0.01 ML Pt coverage). TPD traces for CO ( $m/z = 28$ , red) and  $H_2$  ( $m/z = 2$ , blue) for adsorption of A) 50 L  $H_2$ , B) 0.2 L CO, C) 0.2 L CO followed by 50 L  $H_2$  D) 50 L  $H_2$  followed by > 0.2 L CO.

Exploring the impact of CO adsorption on the uptake and release of  $H_2$ , we find that when we do not expose 0.01 monolayer (ML) PtCu(111) SAA to any CO,  $H_2$  desorbs from the surface at 250 K (**Figure 1A**). The higher desorption temperature observed in this current study is due to the presence of CO on some Pt sites as discussed below. Notably, while we did not introduce CO deliberately in this case, adsorption of small amounts of CO always present in the background of the UHV chamber causes occupation of some Pt sites, as evidenced by a small area CO peak centered at 350 K (**Figure 1A**). Additional CO exposure of greater than 0.2 L at 85 K saturates the Pt sites (0.01 ML) with CO while producing a low coverage of excess CO on the Cu terraces (0.03 ML) (**Figure 1B**). Our desorption traces are in agreement with previous studies

that show CO desorbing from Cu(111) terraces at 170 K for CO coverages below saturation and 200 K from Cu steps.<sup>17, 20, 40</sup> When we co-adsorb H<sub>2</sub> and CO, the desorption traces are dependent on the order of gas exposure. If CO is adsorbed prior to H<sub>2</sub> exposure, we do not observe any uptake of H (**Figure 1C**). CO blocks the Pt sites, inhibiting the dissociation of H<sub>2</sub>, despite the availability of Cu sites. When we adsorb H<sub>2</sub> prior to CO, we observe H<sub>2</sub> desorption at 285 K, 55 K higher than the desorption temperature of H<sub>2</sub> on PtCu SAAs without CO exposure.

Intriguingly, and unlike the case of PdCu SAAs, the H<sub>2</sub> recombination on PtCu SAAs appears to begin prior to desorption of CO from Pt sites (**Figure 1D**). Furthermore, we observe that the full-width-half-max of the H<sub>2</sub> desorption peak decreases from 35 K to 25 K in the presence of CO, suggesting that CO traps H on the surface by blocking a low temperature desorption pathway and allows it to acquire more energy at elevated temperatures and desorb at a faster rate.

### **H/CO Atomic-Scale Adsorption Site Preference**

The interaction of CO and H with the Pt active sites was directly probed through molecular manipulation experiments with the LT-STM tip (**Figure 2 A-G**). As shown in **Figure 2A**, the Pt atoms are well dispersed in the Cu surface and appear in topographic STM images ~20 pm higher than the surrounding Cu lattice. H<sub>2</sub> followed by CO were co-adsorbed onto a 0.01 ML PtCu(111) surface at 85 K before being cooled to 5 K for imaging. We initially observed H adatoms as clusters of mobile depressions on the Cu terraces (**Figure 2B-E**). Previously, we have shown that H adatoms that have spilled over from the dissociation site are mobile on Cu(111) at 5 K due to quantum tunneling through the diffusion barrier (which we calculate using DFT to be 0.13 eV).<sup>21</sup> We then deliberately and selectively remove H adatoms from the imaging window by applying a 200 mV bias to the STM tip while scanning. This causes all the H adatoms to diffuse away, but a few immobile depressions remain on the surface (**Figure 2F**), which require a high

(5 V) local pulse to remove. It is well established that  $\geq 2.4$  V pulses are needed to desorb CO atoms from metallic surfaces,<sup>41</sup> therefore we identify those immobile depressions in **Figure 2F** as CO molecules. Directly underneath the CO molecules we observed stationary surface protrusions  $\sim 20$  pm in apparent height, which are the Pt atoms substituted into the Cu lattice (**Figure 2G**). These results demonstrate the preferred adsorption sites of CO molecules are the isolated Pt atoms and that surface H resides on the Cu(111) surface.

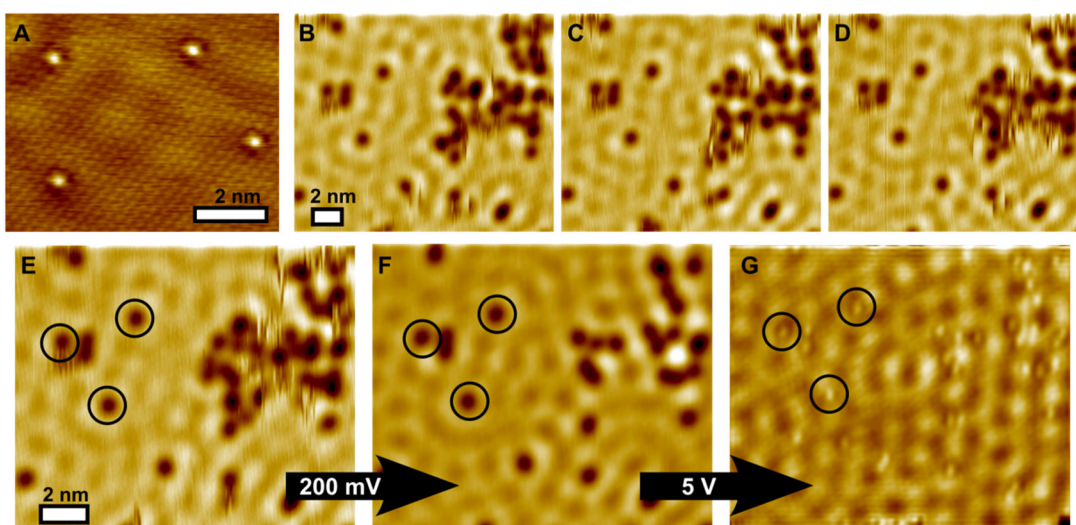


**Figure 2.** STM images of the co-adsorption of H and CO on 0.01 ML PtCu(111) SAAs. A) Atomic resolution STM image of individual isolated Pt atoms in Cu(111). Imaging conditions: 10 mV 150 nA. B-D) Time-lapse images of adsorbed H and CO showing H atom diffusion (vertical streaks) and stationary CO. Imaging conditions: 30 pA and 30 mV. E-G) STM manipulation experiments that remove the mobile H atoms and show the Pt active site. E) STM image after adsorption of H and CO. F) Image after 200 mV scan to remove adsorbed H atoms from imaging frame. G) Image after local 5 V pulses to remove adsorbed CO revealing a Pt atom under each CO molecule. Three Pt sites are highlighted with circles. The images B-F) were taken at 30 mV and 30 pA and image G) 10 mV and 50 nA.

### DFT Calculations of CO and H<sub>2</sub> Adsorption/Desorption Mechanisms

In order to elucidate the unusual desorption behavior of H<sub>2</sub> in the presence of CO on the PtCu(111) SAA surface we perform DFT calculations. We evaluate the binding strength of each of these species as well as their mechanisms of adsorption and desorption on the various site types of both surfaces. Finally, using DFT we consider whether H-H recombination via single Pt atoms in PtCu(111) SAA is possible whilst CO is still adsorbed, and evaluate the mobility of adsorbed H and CO by calculating diffusion barriers.

The adsorption energies of a single H adatom on shared Pt-Cu-Cu fcc and hcp SAA sites are -0.14 eV and -0.16 eV, respectively (**Figure 3A**). The adsorption of H on SAA sites is slightly stronger than on pure Cu fcc and hcp sites, with the adsorption energy of H in either site (on Cu) being -0.09 eV (**Figure 3A**). The similarities in the binding strength, in addition to the low barriers of H adatom surface diffusion and the high multiplicity of Cu sites in a SAA, facilitate the low temperature spillover of H from the single Pt atom to pure Cu, which we have previously observed using STM.<sup>16</sup>

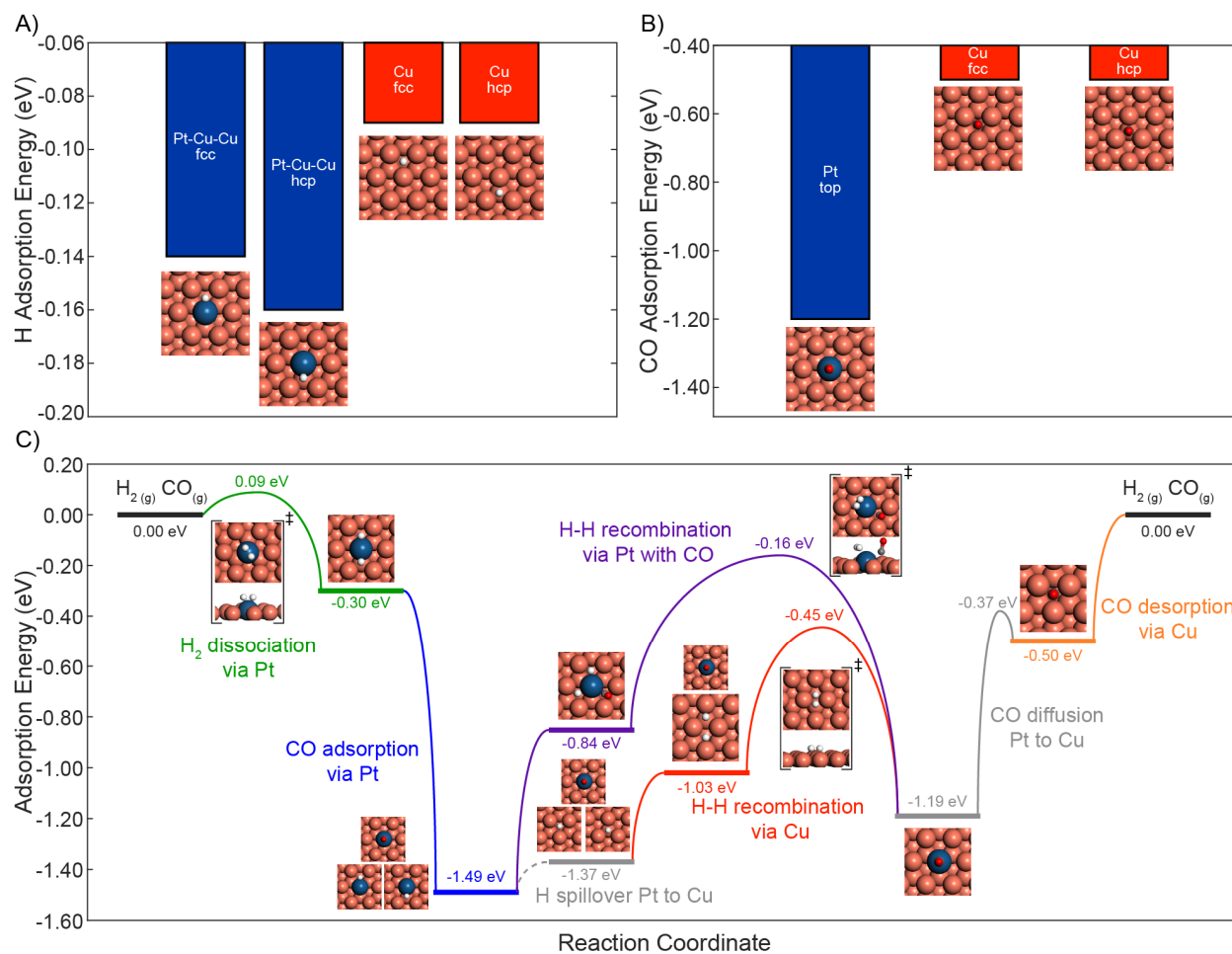


**Figure 3.** Adsorption energy diagrams of A) H adatom binding on shared Pt-Cu-Cu fcc and hcp hollow sites, as well as on threefold Cu fcc and hcp sites; and B) a CO molecule on Pt top site as well as that on Cu fcc and hcp hollow sites. Panel C) gives the adsorption energy as a function of reaction coordinate showing H<sub>2</sub> adsorption at isolated Pt atoms (green), CO adsorption at isolated Pt atoms (blue), H-H recombination at isolated Pt atoms with CO co-adsorbed (purple), H-H recombination on pure Cu (red) and CO desorption from pure Cu (orange). Diffusive steps are shown in grey. Transition state structures are encased in brackets and denoted by ‡. Stable states are given by horizontal lines on the energy diagram where multiple structures indicate adsorbates at infinite separation.

The mechanism for H<sub>2</sub> dissociation on the PtCu(111) SAA proceeds via the single Pt atom top site (**Figure 3C**). This is consistent with *ab initio* studies of H<sub>2</sub> dissociation on PdCu(111) SAAs

and with our previous work using a different computational setup.<sup>42-44</sup> The two resulting H atoms bind to Pt-Cu-Cu fcc and hcp hollow sites that are separated by the Pt atom; this configuration has a total adsorption energy of -0.30 eV, indicating a negligible interaction between the two H adatoms. The total barrier for the recombination of the two H adatoms on the SAA surface is 0.39 eV compared to 0.92 eV on Cu(111) (**Figure 3C**, reverse green pathway and red pathway, respectively). Hence, we observe low temperature desorption at 230 K from the PtCu(111) SAA, that is 70 K lower than from pure Cu(111).<sup>16, 38</sup>

Considering the adsorption of CO on pure Cu(111), we find that CO is most stable in threefold fcc and hcp sites with an adsorption energy of -0.50 eV (**Figure 3B**). On the PtCu(111) SAA, CO binds most favorably to single Pt atom top sites with an adsorption energy of -1.19 eV (**Figure 3C**); in fact, any attempts to optimize the structure of CO in shared PtCu sites result in relaxation to the Pt top site. These adsorption energies are in good agreement with our STM experiments, by which we concluded that CO preferentially binds to isolated Pt atoms in PtCu(111) SAA, rather than on facets of pure Cu(111) (**Figure 2F**). We correctly predict the most favorable adsorption site on the PtCu(111) SAA, however on Cu(111), experiment shows that CO is most stable on Cu top sites. A lack of qualitative agreement for CO adsorption site preference on Cu(111) is a well-documented issue when employing DFT calculations under the generalized gradient approximation and we take this opportunity to refer the reader to interesting discussions by Kresse *et al.*<sup>45</sup> and Feibelman *et al.*<sup>46</sup> that allude to the origins of the apparent contradiction to experimental works. Despite the site preference issues, we point out that the RPBE xc-functional employed here is specifically designed to reliably reproduce the CO adsorption energy.<sup>27</sup> Indeed, with a similar set-up to that employed in this study, we have used

DFT with RPBE to obtain CO adsorption energies on an assortment of SAA and pure metal surfaces with a mean absolute error of 0.04 eV when compared to experiment.<sup>29</sup>

A recent study by Thirumalai and Kitchin related the electronic structure of SAAs to their reactivity.<sup>47</sup> Through analysis of the atom-projected d-band density of states (PDOS) of a number of SAAs, it was determined that there is poor charge mixing between isolated platinum group metal atoms and their coinage metal host matrices.<sup>47</sup> This results in a sharp peak in each dopant PDOS close to the Fermi level that is akin to that of an isolated gas phase dopant atom.<sup>47</sup> Thus, these isolated dopant sites are highly reactive, explaining the low activation barrier we calculated for H-H recombination and H<sub>2</sub> dissociation over Pt sites in PtCu(111) SAAs. Indeed, in a broad theoretical survey of SAA reactivity we showed that SAA materials exhibit enhanced reactivity in numerous adsorption and bond scission reactions relevant to catalysis.<sup>44</sup>

Computing the adsorption energy of H and CO that are co-adsorbed at a single Pt atom on the PtCu(111) SAA surface, we find that the interaction of these two adspecies is highly repulsive. In order to co-adsorb at an isolated Pt atom, H binds on a shared Pt-Cu-Cu fcc/hcp site whereas CO is heavily displaced from the Pt atom top site due to the strong repulsive interaction (0.37 eV) exerted between these two species. The addition of a second adsorbed H adatom on the isolated Pt atom further destabilizes the adsorption by 0.27 eV (**Figure 3C**, co-adsorbed CO+2H configuration at -0.84 eV, 0.64 eV higher than the infinitely separated configuration of these three molecules). This unstable configuration serves as the initial state for H-H recombination in the presence of CO adsorbed to Pt, though we compute a total activation barrier of 1.34 eV from infinite separation (**Figure 3C**, from blue state via purple pathway). Notably, this total barrier, accounting for the energy required to overcome strong repulsive lateral interactions between CO and H, is much greater than the total desorption barrier from PtCu(111) via Cu sites of 1.04 eV



(**Figure 3C**, from blue state via red pathway). Thus, the desorption of H<sub>2</sub> from a CO-covered site is not likely and the corking effect of CO persists on the PtCu(111) SAA.

In search of another explanation for the experimental results that show hydrogen desorbing prior to CO, we examined the mobility of CO adspecies on the surface, considering the possibility that CO migration might transiently free Pt sites and enable H<sub>2</sub> desorption. To this end, we computed the minimum energy pathway for the CO diffusion between Pt and Cu on the PtCu(111) SAA surface. The pertinent transition state is located on the bridge site between two Pt first nearest neighbor Cu atoms and the corresponding activation barrier is 0.83 eV (**Figure 3C**, grey pathway on the right), which is 0.10 eV less than the H<sub>2</sub> desorption barrier on Cu(111) and 0.51 eV greater than the PtCu(111) H-H recombination barrier in the absence of CO. These data provide a useful starting point for KMC simulations that probe the mechanism of the punctured cork effect.

### **KMC Simulated Thermal Desorption Spectra**

Parameterized by data from our DFT calculations, we use KMC to simulate the TPD of H<sub>2</sub> and of CO from Cu(111) and PtCu(111) SAA, as well as both species together from PtCu(111) SAA. In the case of H<sub>2</sub> TPD from Cu(111) (**Figure 4A**), our simulations yield a peak desorption temperature of 312 K with a half-peak maximum width of 35 K. This simulated TPD profile is in excellent agreement with experimental H<sub>2</sub> TPD from Cu(111) by Anger *et al.* (315 K).<sup>38</sup> For H<sub>2</sub> desorption from PtCu(111) SAA (**Figure 4B**) we achieve good qualitative agreement with experiment as the simulated TPD peak temperature is low (165 K) compared to that from Cu(111), though is a 65 K underestimation compared to our experiment (**Figure 1A**). Analysis of

the reaction statistics shows that the low temperature desorption of H<sub>2</sub> from PtCu(111) SAA (**Figure 4B**) is solely due to H-H recombination via single Pt atoms.

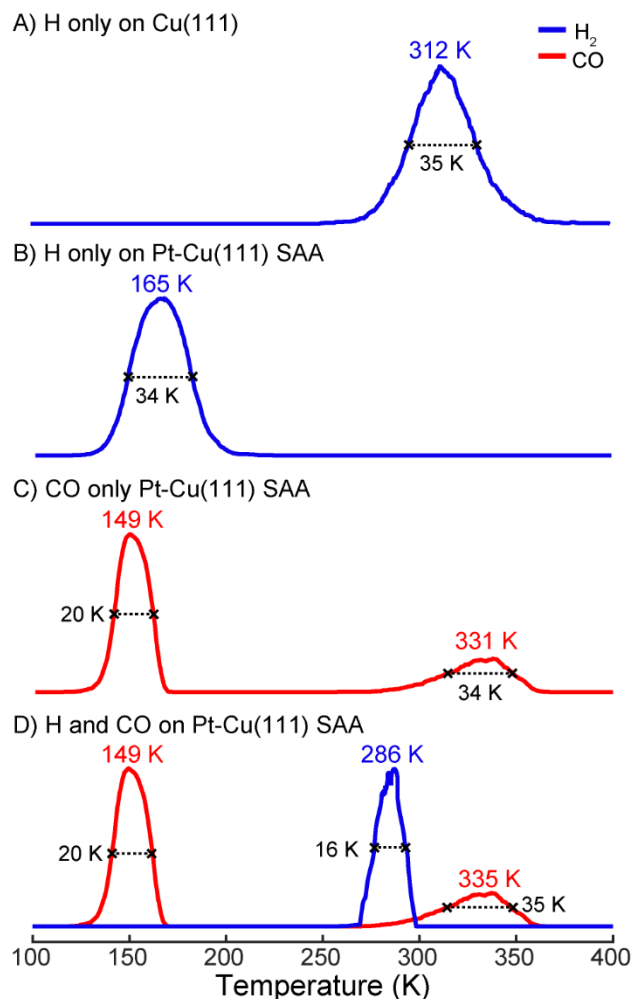


**Figure 4.** KMC simulated TPD traces of (A) H<sub>2</sub> from Cu(111) using an initial H surface coverage of 0.33 ML; (B) H<sub>2</sub> from PtCu(111) SAA using an initial H surface coverage of 0.33 ML; (C) H<sub>2</sub> from PtCu(111) SAA using an initial H surface coverage of 0.33 ML and CO coverage of 0.33 ML; and (D) CO from PtCu(111) SAA using an initial CO surface coverage of 0.33 ML. The temperature in each simulation was raised from 100 K to 400 K at a ramp rate of 1 K·s<sup>-1</sup>, using CO and H<sub>2</sub> partial pressures of 0 to reproduce UHV conditions. H<sub>2</sub> TPD traces are shown in blue whereas that for CO is shown in red.

In the case of CO TPD, our simulations yield peak desorption temperatures of 149 K and 331 K from PtCu(111) SAA (**Figure 4C**) which compare well with the peaks at 160 K and 350 K recorded experimentally (**Figure 1B**). Notably, we do not reproduce the secondary CO desorption peak at 200 K in our simulations as we do not explicitly model CO desorption from Cu step edges but rather (111) terrace sites exclusively. Reaction statistics from the KMC simulation show that the peak at 149 K can be attributed to CO desorption from Cu sites within the SAA. This is in good agreement with our assignment of the low temperature peak in **Figure 1B** (160 K) that was made based on previous TPD studies on pure Cu(111).<sup>17, 20, 40</sup> According to the reaction statistics the secondary peak at 331 K corresponds to desorption from both Cu and Pt sites, though the number of CO species evolved is equivalent to the total number of Pt sites. When there is a stoichiometric amount of CO molecules adsorbed at the Pt sites and the temperature is below 250 K, such that CO cannot diffuse away from Pt, all Pt atoms will be saturated and no CO will be present on Cu. Above this temperature, there is sufficient thermal energy for CO to overcome diffusion barriers of 0.83 eV and 0.85 eV in order to move away from Pt onto Cu sites whereon, due to the high multiplicity of these sites, it may temporarily stay until a vacant Pt site is found. The residence time of CO on Cu is short, though on a timescale comparable to the kinetic constant for CO desorption from Cu at this temperature, allowing CO to desorb from the surface via these sites rather than directly from Pt. Interestingly in our simulations, CO diffusion remains in quasi-equilibrium throughout, specifically because the CO desorption via Cu occurs on a much slower timescale than CO diffusion from Pt to Cu. This is evidenced by three orders of magnitude of difference between their respective rates and effectively quasi-equilibrates the Pt to Cu CO diffusion (see supporting information). A mechanism of diffusion followed by desorption from weaker binding sites is somewhat unusual

though has previously been used in the successful interpretation of spectra for the TPD of aromatic compounds from vicinal Cu(433).<sup>48</sup> In this case, benzene and naphthalene freely migrate from strong binding Cu(433) steps to weak binding Cu(111) terraces, well below the onset of desorption and cooperative desorption from both surfaces gives rise to a broad high temperature peak,<sup>48</sup> analogous to that which we observe in our study (**Figure 1B** and **Figure 4C**).

Before we discuss simulations of the co-adsorbed system, we briefly remark on the reliability of our simulations this far. For the single-adsorbate systems, we have very good agreement between our simulated TPD spectra and experiment for H on Cu(111), CO on Cu(111) and CO on PtCu(111) SAA, though for H on PtCu(111) we have only qualitative agreement. Our DFT calculations predict a low H<sub>2</sub> dissociation barrier of 0.09 eV, which agrees well with our experimental observation that PtCu(111) SAA can activate H<sub>2</sub> at temperatures < 85 K. Thus, as the H-H recombination barrier is a sum of the dissociation barrier and the adsorption energy of two H adatoms, we infer that our DFT calculations must under-predict the binding strength of H on Pt sites. We used the RPBE functional that is specifically designed to overcome common issues of over-binding, though in the case of H adsorption this compensation appears to be too great.

In our previous work<sup>44</sup> using the OptB86b-vdW<sup>49</sup> functional, we found comparable PtCu(111) SAA H<sub>2</sub> dissociative adsorption barriers to RPBE, though more negative adsorption energy of H (-0.29 eV). Using this adsorption energy in our TPD simulation, results in a peak desorption temperature of 218 K that is in much better agreement with the experimental TPD peak of 230 K (**Figure 1A**). Unfortunately, this functional heavily over-binds CO (-1.61 eV), and as a result the simulated CO TPD peak temperature is predicted to be >100 K too high. This is problematic for

studying the co-adsorbed system as, during the KMC TPD simulation, H<sub>2</sub> evolves from the surface via Cu sites at a desorption temperature of 312 K irrespective of the presence or absence of CO and is therefore qualitatively incorrect compared to what we observe experimentally (**Figure 1D**). Thus, despite a lack of quantitative agreement with experiment for the desorption of H<sub>2</sub> from PtCu(111) SAA when using RPBE, we recognize that the H-H recombination must be rate-limited by the presence of CO and therefore we choose the RPBE functional to model the co-adsorbed system as it gives the best representation of the CO desorption kinetics.

In the co-adsorbed H<sub>2</sub> and CO system on PtCu(111) (**Figure 4D**), we simulate a peak desorption temperature of H<sub>2</sub> that has increased to 286 K compared to in the absence of CO. The CO desorption trace is very similar to that in the absence of H adatoms. Closer inspection of the reaction statistics (**Figure 5**) reveals that some H<sub>2</sub> leaks slowly from the surface via Cu sites when there is a stoichiometric 1:1 amount of CO to Pt. Notably, no desorption of H<sub>2</sub> via Pt is simulated until CO desorption occurs. Heating the system is essential to facilitate CO desorption which, at the start of the temperature ramp (100 K), will occur from Pt on the timescale of  $1.22 \times 10^{42}$  s or  $3.87 \times 10^{34}$  years ( $k_{100\text{K}} = 8.20 \times 10^{-43}$  s<sup>-1</sup>). However, once sufficient thermal energy is attained, such that a single CO molecule desorbs (making the CO:Pt ratio sub-stoichiometric), H-H recombination is facile and rapid via unoccupied Pt sites. This fast desorption of H<sub>2</sub> is reflected by a narrowing in the half-peak maximum width from 34 K in the absence of CO to 16 K in the presence of CO (**Figure 4B** and **D**, respectively). Analyzing the reaction statistics (**Figure 5**) shows that the majority of H<sub>2</sub> desorbs via Pt sites. Moreover, they show that the sharpness in the H<sub>2</sub> desorption peak is due to the CO site blocking causing H adatoms to be trapped on the surface well above the activation required for normal H-H recombination at Pt sites.

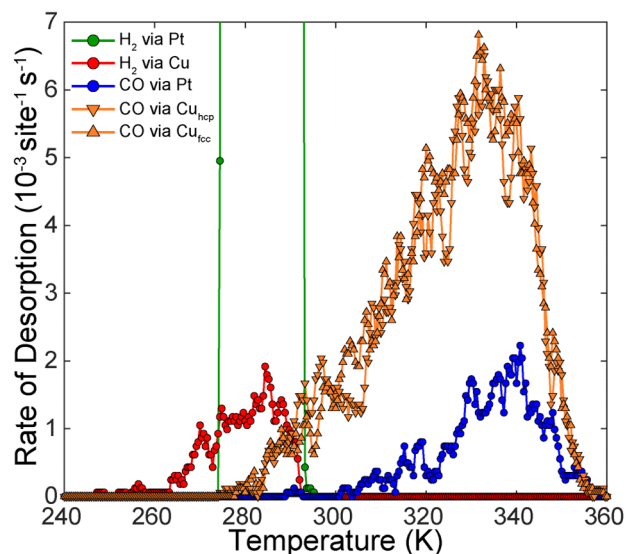


**Figure 5.** Desorption rates as functions of temperature during KMC simulated TPD on PtCu(111) SAA for the desorption of H<sub>2</sub> via Pt sites (green), H<sub>2</sub> via Cu (red), CO via Pt (blue), CO via Cu hcp sites (orange, inverted triangle) and CO via Cu fcc sites (orange, triangle); note that the “Rate of Desorption” scale is adjusted to more clearly show the dependence of H<sub>2</sub> desorption via Pt on the desorption of CO thereby clipping the peak of the former (at 286 K) from the figure.

Interestingly, by the time the H<sub>2</sub> peak maximum is reached, only 0.7 % of CO has desorbed from the surface indicating that very few Pt sites need to be free to facilitate fast H-H recombination. In fact, we initialize several simulations with sub-stoichiometric coverage of CO to Pt and note a non-linear dependence of the H<sub>2</sub> desorption peak temperature depending on the percentage of Pt atoms covered by CO (**Figure 6A** and **B**). Similarly in experiment, we observe a shifting TPD trace for H<sub>2</sub> desorption that is dependent on CO exposure. Exposures of greater than 0.2 L up to 2.0 L of CO result in the same desorption spectrum shown in **Figure 1D** (**Figure 6C**) indicating that the Pt is saturated by CO over this interval. At lower exposures we find that the H<sub>2</sub> desorption peak temperature takes intermediate values between the cases when only background CO is present and when the surface is saturated with CO (**Figure 6C**).

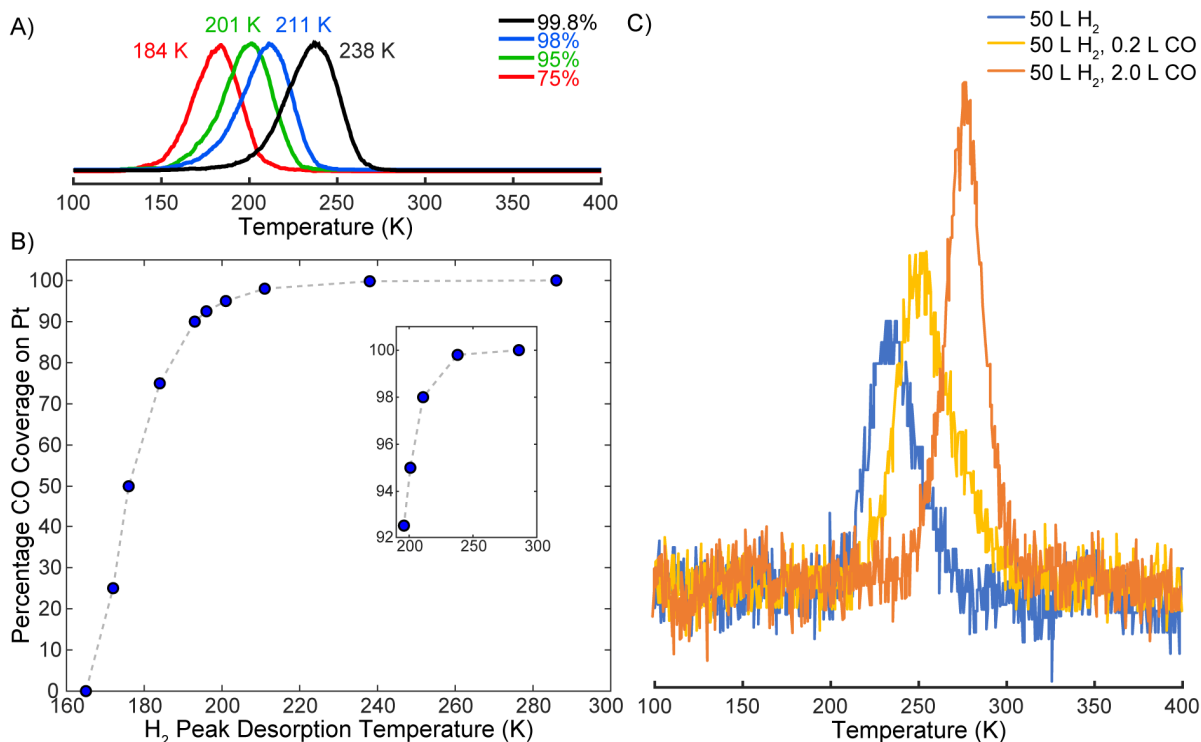


**Figure 6.** KMC simulated TPD of H<sub>2</sub> from the PtCu(111) SAA with varied CO percentage coverage on Pt, showing A) profiles for H<sub>2</sub> desorption at 99.8 % (black), 98 % (blue), 95 % (green) and 75 % (red) Pt covered by CO at initialization and B) plot of Pt atom percentage coverage by CO vs. H<sub>2</sub> peak desorption temperature with inset magnified to show higher temperature region; C) corresponding experimental H<sub>2</sub> TPD after 50 L of H<sub>2</sub> exposure followed by 0 L, 0.2 L and 2 L of CO exposure.

The simulated non-linear dependence of the H<sub>2</sub> desorption peak temperature with CO coverage shown in **Figure 6B** suggests that the most drastic effect on H-H recombination is at high CO exposure, where the majority of Pt sites are blocked. Indeed, having just 0.2 % of Pt atoms free is enough to reduce the H<sub>2</sub> desorption peak temperature by 48 K. Recalling our simulation of CO TPD on PtCu(111) SAA shown in **Figure 4C**, the leading edge of the CO desorption trace extends to over 80 K below the peak. In the context of our experimental TPD (**Figure 1B**) this would suggest that very small, undetectable amounts of CO begin to desorb from the surface just

below 270 K, coinciding with the start of the sharp H<sub>2</sub> desorption peak. At these elevated temperatures, well above those required for normal H<sub>2</sub> desorption, just these few desorbing CO molecules are, according to our simulations (**Figure 6A and B**), sufficient to allow for fast H-H recombination and desorption, despite a low number of active sites.

In our previous work on the PdCu(111) SAA molecular cork system,<sup>12</sup> the DFT computed adsorption energy of CO on the single Pd atom is -0.84 eV, 0.34 eV stronger binding than to pure Cu (-0.50 eV). The H-H recombination barrier on PdCu(111) SAA is 0.68 eV, 0.16 eV less than the CO desorption barrier from Pd. These calculations are in good agreement with the experimental observation that CO selectively blocks H<sub>2</sub> release at isolated Pd atoms in PdCu(111) SAA, forcing H adatoms to remain on the surface 50 K above their normal desorption temperature.<sup>12</sup> Interestingly in the absence of CO, H<sub>2</sub> desorbs from PdCu(111) SAA with a peak temperature of 210 K<sup>12</sup> which is just 20 K less than on the PtCu(111) SAA surface used in this study. On the other hand, the difference in CO desorption peak temperature is larger, being 270 K on PdCu(111) SAA and 350 K on PtCu(111) SAA. It follows that H adatoms are trapped on the surface by CO in the PtCu(111) SAA system at much higher temperature than in the case of PdCu(111) SAA. Therefore, when CO finally begins to desorb from each surface, H-H recombination is much faster on PtCu(111) SAA than on PdCu(111) SAA as reflected by CO induced 35 K and 20 K reductions in the H<sub>2</sub> desorption half-peak maximum, respectively.

## **Conclusions**

We have used surface science and microscopy techniques in conjunction with theoretical modelling to investigate the adsorption behavior of H and CO on PtCu(111) SAAs. Our TPD experiments show that CO traps H adatoms on the PtCu(111) SAA surface, 55 K beyond the



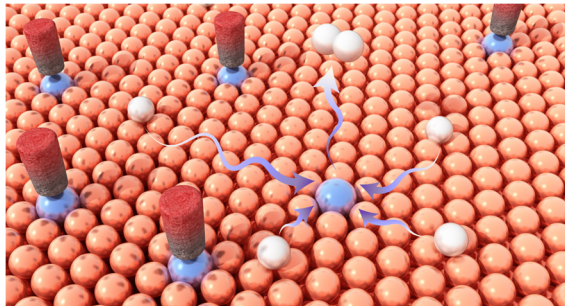
normal H<sub>2</sub> desorption temperature. However, unlike in the PdCu(111) SAA *Molecular Cork* system<sup>12</sup>, we observe experimentally that CO does not desorb prior to H-H recombination. Using high-resolution STM experiments and DFT calculations we show that CO adsorption is specific to single Pt atoms rather than pure Cu(111). Moreover, using KMC we determine that CO is a site blocker for H<sub>2</sub> desorption via single Pt atoms at temperatures up to 55 K beyond the desorption temperature of H<sub>2</sub> in the absence of CO. Analyzing the KMC reaction statistics reveals that some H<sub>2</sub> leaks slowly from surface Cu sites whilst CO molecules are blocking the Pt active sites. However, and most significantly, the majority of H<sub>2</sub> is evolved via recombination at isolated Pt atoms after desorption of the first CO molecule, which explains the experimental results whereby significant H<sub>2</sub> desorption occurs before any CO is detected. We also show that there is a dependence of the H<sub>2</sub> TPD peak temperature on CO exposure and using KMC we determine that this relationship is non-linear with respect to Pt atom CO coverage with the most notable changes occurring just below saturation. This work builds on our discovery of the *Molecular Cork* effect for H<sub>2</sub> evolution from SAAs and demonstrates that a combination of experiment and theory are required to fully understand the interaction of H and CO and their competition for active sites. These important phenomena must be taken into consideration in order for reaction mechanisms on alloy catalysts to be understood.

## **Acknowledgements**

All experimental work (E. C. H. S., Tufts) was supported by the Division of Chemical Sciences, Office of Basic Energy Sciences, CPIMS Program, U.S. Department of Energy, under Grant No. FG02-10ER16170. M. T. D. is supported by the EPSRC Doctoral Prize Fellowship, grant reference number EP/N509577/1. A.M. is supported by the European Research Council (ERC) under the European Union's Seventh Framework Program (FP/2007-2013)/ERC Grant

Agreement 616121 (HeteroIce project). The authors acknowledge the use of the UCL High Performance Computing Facilities (Legion@UCL, Grace@UCL and Thomas@UCL), and associated support services, in the completion of the computational part of this work. We are grateful to the UK Materials and Molecular Modelling Hub for computational resources, which is partially funded by EPSRC (EP/P020194/1). The development of *Zacros* has been funded under the embedded Computer Science and Engineering (eCSE) programme of the ARCHER UK National Supercomputing Service (eCSE01-001, eCSE10-8), as well as by the Leverhulme Trust (RPG-2017-361).

## TOC:



## References

1. Cheng, X.; Shi, Z.; Glass, N.; Zhang, L.; Zhang, J.; Song, D.; Liu, Z.-S.; Wang, H.; Shen, J. A review of PEM hydrogen fuel cell contamination: Impacts, mechanisms, and mitigation. *J. Power Sources* **2007**, *165*, 739-756.
2. Baschuk, J. J.; Li, X. Carbon monoxide poisoning of proton exchange membrane fuel cells. *Int. J. Energy Res.* **2001**, *25*, 695-713.

3. Tang, D. C.; Hwang, K. S.; Salmeron, M.; Somorjai, G. A. High Pressure Scanning Tunneling Microscopy Study of CO Poisoning of Ethylene Hydrogenation on Pt(111) and Rh(111) Single Crystals. *J. Phys. Chem. B* **2004**, *108*, 13300-13306.
4. Montano, M.; Bratlie, K.; Salmeron, M.; Somorjai, G. A. Hydrogen and Deuterium Exchange on Pt(111) and Its Poisoning by Carbon Monoxide Studied by Surface Sensitive High-Pressure Techniques. *J. Am. Chem. Soc.* **2006**, *128*, 13229-13234.
5. Johansson, M.; Lytken, O.; Chorkendorff, I. The sticking probability for H<sub>2</sub> in presence of CO on some transition metals at a hydrogen pressure of 1bar. *Surf. Sci.* **2008**, *602*, 1863-1870.
6. Wang, H.; Tobin, R. G.; Lambert, D. K. Coadsorption of hydrogen and CO on Pt(335): Structure and vibrational Stark effect. *J. Chem. Phys.* **1994**, *101*, 4277-4287.
7. Hoge, D.; Tüshaus, M.; Bradshaw, A. M. Island formation during CO/H coadsorption on Pt{111} studied by IR reflection-absorption spectroscopy. *Surf. Sci.* **1988**, *207*, L935-L942.
8. Calaza, F.; Stacchiola, D.; Neurock, M.; Tysoe, W. T. Coverage Effects on the Palladium-Catalyzed Synthesis of Vinyl Acetate: Comparison between Theory and Experiment. *J. Am. Chem. Soc.* **2010**, *132*, 2202-2207.
9. Richter, L. J.; Gurney, B. A.; Ho, W. The influence of adsorbate-adsorbate interactions on surface structure: The coadsorption of CO and H<sub>2</sub> on Rh(100). *J. Chem. Phys.* **1987**, *86*, 477-490.
10. Lewis, E. A.; Le, D.; Jewell, A. D.; Murphy, C. J.; Rahman, T. S.; Sykes, E. C. H. Visualization of Compression and Spillover in a Coadsorbed System: Syngas on Cobalt Nanoparticles. *ACS Nano* **2013**, *7*, 4384-4392.

11. Morkel, M.; Rupprechter, G.; Freund, H.-J. Ultrahigh vacuum and high-pressure coadsorption of CO and H<sub>2</sub> on Pd(111): A combined SFG, TDS, and LEED study. *J. Chem. Phys.* **2003**, *119*, 10853-10866.
12. Marcinkowski, M. D.; Jewell, A. D.; Stamatakis, M.; Boucher, M. B.; Lewis, E. A.; Murphy, C. J.; Kyriakou, G.; Sykes, E. C. H. Controlling a spillover pathway with the molecular cork effect. *Nat. Mater.* **2013**, *12*, 523-528.
13. Ogura, S.; Okada, M.; Fukutani, K. Near-Surface Accumulation of Hydrogen and CO Blocking Effects on a Pd–Au Alloy. *J. Phys. Chem. C* **2013**, *117*, 9366-9371.
14. Lucci, F. R.; Darby, M. T.; Mattera, M. F. G.; Ivimey, C. J.; Therrien, A. J.; Michaelides, A.; Stamatakis, M.; Sykes, E. C. H. Controlling Hydrogen Activation, Spillover, and Desorption with Pd–Au Single-Atom Alloys. *J. Phys. Chem. Lett.* **2016**, *7*, 480-485.
15. Lucci, F. R.; Liu, J.; Marcinkowski, M. D.; Yang, M.; Allard, L. F.; Flytzani-Stephanopoulos, M.; Sykes, E. C. H. Selective hydrogenation of 1,3-butadiene on platinum–copper alloys at the single-atom limit. *Nat. Commun.* **2015**, *6*, 8550.
16. Lucci, F. R.; Marcinkowski, M. D.; Lawton, T. J.; Sykes, E. C. H. H<sub>2</sub> Activation and Spillover on Catalytically Relevant Pt–Cu Single Atom Alloys. *J. Phys. Chem. C* **2015**, *119*, 24351-24357.
17. Liu, J.; Lucci, F. R.; Yang, M.; Lee, S.; Marcinkowski, M. D.; Therrien, A. J.; Williams, C. T.; Sykes, E. C. H.; Flytzani-Stephanopoulos, M. Tackling CO Poisoning with Single-Atom Alloy Catalysts. *J. Am. Chem. Soc.* **2016**, *138*, 6396-6399.
18. Pedersen, M. Ø.; Helveg, S.; Ruban, A.; Stensgaard, I.; Lægsgaard, E.; Nørskov, J. K.; Besenbacher, F. How a gold substrate can increase the reactivity of a Pt overlayer. *Surf. Sci.* **1999**, *426*, 395-409.

19. Eyrich, M.; Diemant, T.; Hartmann, H.; Bansmann, J.; Behm, R. J. Interaction of CO with Structurally Well-Defined Monolayer PtAu/Pt(111) Surface Alloys. *J. Phys. Chem. C* **2012**, *116*, 11154-11165.
20. Raval, R.; Parker, S. F.; Pemble, M. E.; Hollins, P.; Pritchard, J.; Chesters, M. A. FT-RIRS, XPS and LEIS studies of the adsorption of carbon monoxide on Cu(111). *Surf. Sci.* **1988**, *203*, 353-377.
21. Jewell, A. D.; Peng, G.; Mattera, M. F. G.; Lewis, E. A.; Murphy, C. J.; Kyriakou, G.; Mavrikakis, M.; Sykes, E. C. H. Quantum Tunneling Enabled Self-Assembly of Hydrogen Atoms on Cu(111). *ACS Nano* **2012**, *6*, 10115-10121.
22. Lauhon, L. J.; Ho, W. Direct Observation of the Quantum Tunneling of Single Hydrogen Atoms with a Scanning Tunneling Microscope. *Phys. Rev. Lett.* **2000**, *85*, 4566-4569.
23. Kresse, G.; Furthmüller, J. Efficient iterative schemes for ab initio total-energy calculations using a plane-wave basis set. *Phys. Rev. B* **1996**, *54*, 11169-11186.
24. Kresse, G.; Furthmüller, J. Efficiency of ab-initio total energy calculations for metals and semiconductors using a plane-wave basis set. *Comput. Mater. Sci.* **1996**, *6*, 15-50.
25. Kresse, G.; Joubert, D. From ultrasoft pseudopotentials to the projector augmented-wave method. *Phys. Rev. B* **1999**, *59*, 1758-1775.
26. Blöchl, P. E. Projector augmented-wave method. *Phys. Rev. B* **1994**, *50*, 17953-17979.
27. Hammer, B.; Hansen, L. B.; Nørskov, J. K. Improved adsorption energetics within density-functional theory using revised Perdew-Burke-Ernzerhof functionals. *Phys. Rev. B* **1999**, *59*, 7413-7421.
28. Perdew, J. P.; Burke, K.; Ernzerhof, M. Generalized Gradient Approximation Made Simple. *Phys. Rev. Lett.* **1996**, *77*, 3865-3868.

29. Darby, M. T.; Sykes, E. C. H.; Michaelides, A.; Stamatakis, M. Carbon Monoxide Poisoning Resistance and Structural Stability of Single Atom Alloys. *Top. Catal.* **2018**, *61*, 428-438.
30. Henkelman, G.; Jónsson, H. A dimer method for finding saddle points on high dimensional potential surfaces using only first derivatives. *J. Chem. Phys.* **1999**, *111*, 7010-7022.
31. Stamatakis, M.; Chen, Y.; Vlachos, D. G. First-Principles-Based Kinetic Monte Carlo Simulation of the Structure Sensitivity of the Water–Gas Shift Reaction on Platinum Surfaces. *J. Phys. Chem. C* **2011**, *115*, 24750-24762.
32. Stamatakis, M.; Vlachos, D. G. A graph-theoretical kinetic Monte Carlo framework for on-lattice chemical kinetics. *J. Chem. Phys.* **2011**, *134*, 214115.
33. Nielsen, J.; d’Avezac, M.; Hetherington, J.; Stamatakis, M. Parallel kinetic Monte Carlo simulation framework incorporating accurate models of adsorbate lateral interactions. *J. Chem. Phys.* **2013**, *139*, 224706.
34. Stamatakis, M.; Vlachos, D. G. Unraveling the Complexity of Catalytic Reactions via Kinetic Monte Carlo Simulation: Current Status and Frontiers. *ACS Catal.* **2012**, *2*, 2648-2663.
35. Lucci, F. R.; Lawton, T. J.; Pronschinske, A.; Sykes, E. C. H. Atomic Scale Surface Structure of Pt/Cu(111) Surface Alloys. *J. Phys. Chem. C* **2014**, *118*, 3015-3022.
36. Chatterjee, A.; Voter, A. F. Accurate acceleration of kinetic Monte Carlo simulations through the modification of rate constants. *J. Chem. Phys.* **2010**, *132*, 194101.
37. Stamatakis, M.; Vlachos, D. G. Equivalence of on-lattice stochastic chemical kinetics with the well-mixed chemical master equation in the limit of fast diffusion. *Comput. Chem. Eng.* **2011**, *35*, 2602-2610.

38. Anger, G.; Winkler, A.; Rendulic, K. D. Adsorption and desorption kinetics in the systems H<sub>2</sub>/Cu(111), H<sub>2</sub>/Cu(110) and H<sub>2</sub>/Cu(100). *Surf. Sci.* **1989**, *220*, 1-17.
39. Collins, D. M.; Spicer, W. E. The adsorption of CO, O<sub>2</sub>, and H<sub>2</sub> on Pt: I. Thermal desorption spectroscopy studies. *Surf. Sci.* **1977**, *69*, 85-113.
40. Kirstein, W.; Krüger, B.; Thieme, F. CO adsorption studies on pure and Ni-covered Cu(111) surfaces. *Surf. Sci.* **1986**, *176*, 505-529.
41. Bartels, L.; Meyer, G.; Rieder, K. H.; Velic, D.; Knoesel, E.; Hotzel, A.; Wolf, M.; Ertl, G. Dynamics of Electron-Induced Manipulation of Individual CO Molecules on Cu(111). *Phys. Rev. Lett.* **1998**, *80*, 2004-2007.
42. Kyriakou, G.; Davidson, E. R. M.; Peng, G.; Roling, L. T.; Singh, S.; Boucher, M. B.; Marcinkowski, M. D.; Mavrikakis, M.; Michaelides, A.; Sykes, E. C. H. Significant Quantum Effects in Hydrogen Activation. *ACS Nano* **2014**, *8*, 4827-4835.
43. Ramos, M.; Martinez, A. E.; Busnengo, H. F. H<sub>2</sub> dissociation on individual Pd atoms deposited on Cu(111). *Phys. Chem. Chem. Phys.* **2012**, *14*, 303-310.
44. Darby, M. T.; Réocreux, R.; Sykes, E. C. H.; Michaelides, A.; Stamatakis, M. Elucidating the Stability and Reactivity of Surface Intermediates on Single-Atom Alloy Catalysts. *ACS Catal.* **2018**, *8*, 5038-5050.
45. Kresse, G.; Gil, A.; Sautet, P. Significance of single-electron energies for the description of CO on Pt(111). *Phys. Rev. B* **2003**, *68*.
46. Feibelman, P. J.; Hammer, B.; Nørskov, J. K.; Wagner, F.; Scheffler, M.; Stumpf, R.; Watwe, R.; Dumesic, J. The CO/Pt(111) Puzzle†. *J. Phys. Chem. B* **2001**, *105*, 4018-4025.
47. Thirumalai, H.; Kitchin, J. R. Investigating the Reactivity of Single Atom Alloys Using Density Functional Theory. *Top. Catal.* **2018**, *61*, 462-474.

48. Camarillo-Cisneros, J.; Liu, W.; Tkatchenko, A. Steps or Terraces? Dynamics of Aromatic Hydrocarbons Adsorbed at Vicinal Metal Surfaces. *Phys. Rev. Lett.* **2015**, *115*, 086101.
49. Klimeš, J.; Bowler, D. R.; Michaelides, A. Van der Waals density functionals applied to solids. *Phys. Rev. B* **2011**, *83*, 195131.